Applied Physics Laboratory
University of Washington

1013 NE 40th Street
Box 355640
Seattle, WA 98105-6698

206-543-1300
FAX 206-543-6785
www.apl.washington.edu

30 December 2020

To: Dr. Kyle Becker
Office of Naval Research (Code 322)
875 North Randolph Street
Arlington, VA 22203-1995

From: Dr. Anatoliy Ivakin, Principal Investigator

Subj: ONR Grant N00014-17-1-2196, "Improving prediction of propagation, scattering and reverberation in the Arctic with application to remote acoustic sensing of sea-ice"

Encl: (1) Final Technical Report
(2) SF298 form

Please see the enclosures listed above for the subject grant, "Improving prediction of propagation, scattering and reverberation in the Arctic with application to remote acoustic sensing of sea-ice". Enclosure (1) is the final report that closes the subject grant, with an attached SF298 form as enclosure (2).

cc: ONR Seattle – Ms. Ozma Ragan (ozma.ragan@navy.mil) and
Ms. Naomi Roberson (naomi.roberson.ctr@navy.mi)
Naval Research Laboratory, Code 5596, reports@library.nrl.navy.mil
Defense Technical Information Center: dtic.belvoir.ecm.mbx.tr@mail.mil
University of Washington – Office of Sponsored Programs Closeout Coordinator
Grant & Contract Closeout Coordinator, APL-UW

2017-2020 ONR joint 322OA and 322AG Core Project Final Report

Improving prediction of propagation, scattering, and reverberation in the Arctic with application to remote acoustic sensing of sea ice

Anatoliy N. Ivakin
Applied Physics Laboratory, University of Washington
1040 NE 40th Street, Seattle WA 98105
Phone: (206) 616-4808, fax: (206) 543-6785
Email: ani@apl.washington.edu

Award Number: N00014-17-1-2196
http://www.apl.uw.edu

Abstract

A long-term goal is to develop an approach for a combined analysis of measured short-range HF ULS echoes and LF long-range transmission loss time series to provide a wide-area synoptic assessment of ice type distribution. This project includes analysis of two datasets. The first one is comprised of a 300 kHz ULS echo time series obtained during ICEX03. Its analysis resulted in a practical algorithm for remotely distinguishing between first year and multi-year ice types. The second dataset represents a 3.5 kHz TL time series measured at a 30m depth / 719m range in a deep (3 km) Arctic ocean during ICEX14. Its analysis resulted in a physics-based model for quantitative interpretation of the entire TL time dependence, including multipath forward propagation signal, affected by ice reflection and refraction in a surface duct, and reverberation coda comprised of bottom and ice reflections and scatterings.

Abbreviations:

HF / MF / LF	high / mid / low frequency
ULS	upward-looking sonar
ICEX03 / ICEX14	Ice Experiment 2003 / 2014
FY / MY	first year / multi-year ice types
TL	transmission loss
ALAS	Arctic Line Arrays System
APLIS	Applied Physics Laboratory Ice Station

LONG-TERM GOALS

This research is aimed to develop a general physics-based modeling approach to acoustic propagation, scattering, and reverberation in the Arctic ocean, with applications to remote acoustic sensing of sea-ice. This includes developing new inversion algorithms for data acquired using high-frequency upward-looking sonar (ULS) for remotely estimating parameters of sea ice, such as thickness, roughness, heterogeneity, and particularly the ice type and age. The physics-based approach will help to better understand mechanisms controlling low-frequency under-ice propagation and reverberation, will improve a theoretical support for experiments in the Arctic and for quantitative interpretation of the data obtained. A general long-term goal is to use understanding developed in this research for a combined analysis of short-range ULS measurements and long-range reverberation data to provide a wide-area synoptic assessment of sea ice physical properties and type/age distribution.

OBJECTIVES

Specific objectives of this research include analysis of two representative datasets. The first one was obtained during ICEX03 using monostatic 300 kHz ULS echo time series, and its analysis is mainly aimed to distinguishing between first year and multi-year ice types. The second dataset was obtained in a deep (3 km) ice-covered environment during ICEX14 using a 3.5 kHz source of opportunity located at a 719m range from receiving system. Its analysis was aimed to better understand mechanisms of MF under-ice reverberation and to suggest a physics-based model for quantitative interpretation of received acoustic intensity time series.

TECHNICAL APPROACH AND WORK COMPLETED

To accomplish the project's goals and objectives, a combined research was performed, which included theoretical time-domain modeling and computer simulations, laboratory physical modeling and experimentation, data analysis and model-data comparisons. In a HF part of the project, a two-scale approach to analysis of ULS echo time series was used assuming incoherent scattering from rough ice. Effects of small-scale "within-footprint" roughness and large-scale "beyond-footprint" ice profile were examined, as well as effects of ULS system parameters, directivity, sonar depth, transmitted pulse shape, chosen thresholds and gains, and others. The ICEX03 ULS data analysis is completed and resulted in suggesting an algorithm for determining the ice type/age based on "local statistics", the mean and standard deviation for draft and echo duration, derived from subsets of echo time series measured along the ULS footprint trajectory. In a MF part of the project, the ICEX14 transmission loss and reverberation data analysis is completed. It is based on a semi-coherent approach accounting for multipath propagation and scattering in the under-ice waveguide. This resulted in developing a unified model for quantitative interpretation of the entire TL time dependence as a whole, including forward propagation signal, affected by ice reflection and refraction in a surface duct, and reverberation coda comprised of bottom and ice reflections and scatterings, with each mechanism dominating within its own time interval. The approach and work completed are described in more detail below for the two parts of the project corresponding to its HF and MF components.

1 HF ULS modeling and data analysis for remote sensing of sea ice

1.1 Introduction

HF ULS systems are commonly used to estimate sea-ice draft and thickness from echo's arrival time [see e.g. Moritz and Ivakin (2012)]. Commonly, only the echo leading edge arrival time (measured at a somewhat arbitrarily chosen detection threshold) is used for this, so most of acoustic raw data, the full echo waveform, in terms of received voltage time series, *V(t)*, normally is not archived. However, the draft profiles estimated from the leading edge are usually biased, with the accuracy and spatial resolution depending on system parameters, such as frequency, directivity, sonar depth, transmitted pulse shape, chosen thresholds and gains, and others. For instance, the horizontal resolution scale is limited by the ULS footprint, which (for commercial HF ULS systems operating typically at 300-500 kHz and ranges 20-60 m), is normally ~ 1-3 m, and the smaller details of the ice draft profile are not resolvable.

This project proposed to analyze the entire echo time series, not only the leading edge, together with in-situ "ice truth" data at ICEX03, and to examine possibilities to infer additional information about ice from such analysis. The proposed technical approach assumes physics-based modeling of various mechanisms of scattering from sea ice, particularly effects of the ice-water interface roughness. The project suggests considering the roughness of different types. First one is the "microroughness" with horizontal scales smaller than a few acoustic wavelengths, i.e. sub-cm scales (at typical ULS frequencies), that can be described by the Bragg scattering mechanism and results in non-specular echo returns from the interface. Of particular interest is roughness of the ice skeletal layer which has vertically oriented elements of a few cm length in depth and horizontal cross-scales typically just a few mm. This type of roughness suggests an incoherent diffuse scattering mechanism. Alternatively, this microroughness can be treated as a thin heterogeneous layer near ice-water interface [Ivakin (1998)]. Another type is the large-scale roughness, or "macro-roughness" that describes the 2D variation of the ice draft/profile. It defines the local slope of the ice profile (and the local incidence angle) on which the micro-roughness is superimposed. The macroroughness can be in turn separated on two parts, the "beyond-footprint" roughness, which is normally given by ULS-measured/resolved ice profiles, and "within-footprint" roughness, which has horizontal scales from a few cm to ~1m and is normally unresolvable.

In this research, modeling of ULS echo intensity time series and numerical simulations were performed for several types of the ice profile [Ivakin (2019)]. The goals were to better understand the bias of the draft derived from the ULS echo measurements and, also, the effects of various system parameters, such as the beam-width and the emitted pulse duration. For instance, the draft estimates inferred from the echo leading edge tend to be biased high because the reflection/scattering from ice tips/ridges (large-scale features of ice "macroroughness"), where the ice thickness has local maxima, arrive earlier than an echo from flat layer of equivalent mass (with averaged over "within-footprint" thickness). And the rougher interface, the greater the bias. Also, the large-scale roughness results in corresponding variations of the draft statistics (for instance, the increase of the draft standard

deviation). Another effect is the increase of the echo duration due to the "within-footprint" roughness and delayed reflection/ scattering from the roughness troughs, where the ice thickness has local minima. This effect is more pronounced for shorter pulses, which therefore are preferable for better estimating the ice roughness.

The effects of some other system parameters were considered as well. For instance, an enhanced receiver gain (or/and a reduced detection threshold) is normally used for emphasizing the echo leading edge that is needed to derive the ice draft from the first crossing of the detection threshold by the echo time series. Because of corresponding saturation effects (tip clipping), this can significantly reduce the value of the measured echo pick's shape and magnitude, whereas the echo duration (that can be estimated using last crossing of the threshold) still can be rather informative. In a simplest example of echoes having a rectangular shape (without any reverberation coda or "tail"), the gain does not affect the echo duration at all. For other shapes, the echo duration becomes sensitive to the system receiver gain. For instance, if echo has a heavy tail, the duration will increase for higher gain, and this can be practically important, particularly in the application to estimating the ice roughness.

Some observations support a sensible assumption that multi-year ice tends to be thicker and more heterogeneous than first-year ice, and the thicker ice is frequently "rougher" than thinner one [e.g., Weeks and Ackley (1986), Frantz et al (2019)]. Our laboratory measurements were aimed to better understand effects of the ice heterogeneity on its acoustic properties. The analysis showed that heterogeneity has a noticeable effect on sound speed and attenuation in the ice [Ivakin et al (2018)]. Also, scattering from the ice heterogeneity within the penetration depth (at near-normal incidence, for the ULS frequencies, on the order of 10 cm) results in a longer tail of the echo comparing to the case of a flat homogeneous ice, thus enhancing a similar effect of ice roughness.

As an application of this research, a new algorithm for ULS data analysis was suggested. The algorithm is based on effects of ice roughness and heterogeneity on the shape of the ULS echo intensity time series and uses the ice draft and echo duration statistics. A simple version of the algorithm was applied to examine ICEX03 APLIS ULS voltage datasets archived in [Moritz (2016)]. It was demonstrated, in particular, that a joint analysis of the locally estimated ice draft mean and standard deviation is capable of providing a quantitative criterium for discriminating between the first year and multi-year ice [Ivakin (2019)].

In more detail, theoretical modeling, computer simulations, laboratory experiments, and data analysis are described in the following sections.

1.2 Modeling approach and computer simulations: effects of ice roughness

We use an approach that, in general, follows a two-scale model of incoherent scattering frequently used, for instance, in geoacoustic modeling and HF acoustics of the seafloor, see e.g. [Jackson and Richardson (2007)] and [Jackson et al (2010)]. Consider time-dependent intensity at a reference distance r_0 from a directional sonar

$$I_0(t) = F(\theta)Q(t - r_0/c)/r_0^2,$$

where $F(\theta)$ is the directivity function for different angles θ off the axis of the sonar beam, $Q(t)$ specifies the radiated signal intensity time-dependence, and c is the sound speed in water. Assume that the scattering interface is given by a superposition of a small-scale random "microroughness" and a background profile that represents "macroroughness". Then the intensity time series of the scattered back to the ULS signal can be written as an incoherent summation or integral over the profile interface as follows

$$I_b(t) = \int F(\theta)Q(t - 2r_\theta/c)P(r_\theta)m_S(\theta')dS_\theta \quad (1)$$

where $P(r)$is a two-way propagation loss factor, r_θ is the slant range between the sonar and the element of profile interface dS_θ for the angle θ, $m_S(\theta')$ is the dimensionless coefficient of local backscatter from microroughness, or the local scattering cross-section per unit surface area, θ' is a local incidence angle, which can differ from θ because of a varying local slope along of the profile interface.

The propagation loss factor accounts here only for the spherical spread and absorption in water and is taken of the form

$$P(r) = (r_0/r)^4 e^{-2\beta r} \quad (2)$$

with β being the absorption coefficient. Various physics-based expressions for the scattering coefficient, m_S, can be found in the literature, see for instance [Jackson et al (2010)] and references therein. A rather general example of an empirical expression for this coefficient is of the form

$$m_S(\theta) = M\,cos^\gamma(\theta) \quad (3)$$

A case with $\gamma = 2$ corresponds to the so-called Lambert scattering rule, which is frequently used for description of diffuse scattering. Here it is exploited to describe scattering from microroughness of the ice-water interface, such as that of the ice skeletal layer, whose elements are vertically oriented having the vertical scale and horizontal cross-scale typically a few cm and a few mm respectively, which suggests a diffuse mechanism of scattering at the ULS frequencies.

Computer simulations for echo intensity time series were performed and analyzed [Ivakin (2019)] to better understand the effects of ice roughness. Equation (1) was used for examining the sensitivity to ULS system parameters, such as frequency, directivity, depth, transmitted pulse shape and duration. The echo intensity time series were investigated for various sea-ice profiles with a primary goal to see the effects of within-footprint macroroughness which, unlike the beyond footprint roughness, normally is not resolved by ULS measurements of the ice draft. Examples of such simulations are presented in **Figure 1** and **Figure 2** for different shapes of the ice profile (macroroughness).

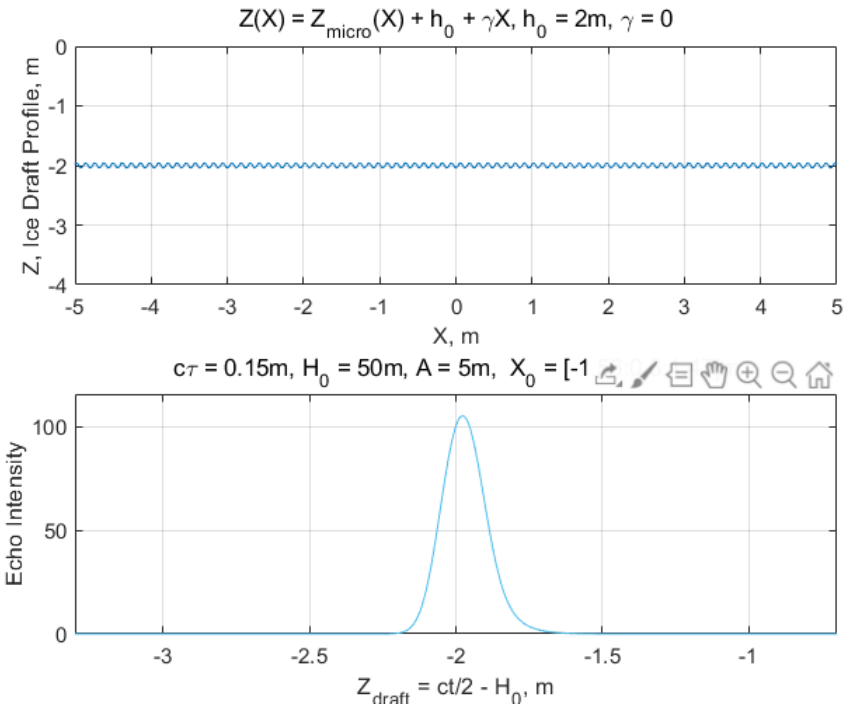

(a)

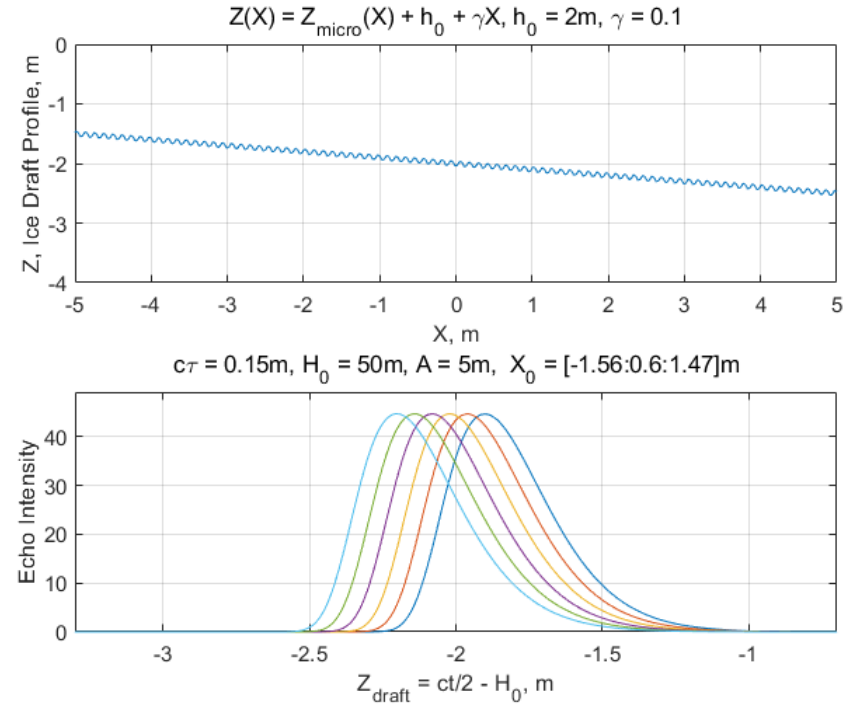

(b)

Figure 1: *Microroughness superimposed on a flat (a) and a linear profile (b), upper subplots, and effect of beyond-footprint macroroughness on the ULS echo time series (lower subplots).*

The ULS parameters are the depth H_0=50m, gaussian half-beam width $\sim 2.5^{\circ}$, which corresponds to footprint size $A = 5$m, and pulse length $c\tau = 15$ cm. The echo intensity time series are shown in the lower parts of each subplot as functions of a scaled time, the instant draft, $Z_{draft} = \frac{ct}{2} - H_0$. Fig.1 corresponds to the case where the footprint is much smaller

than a horizontal scale of macroroughness, i.e. the draft estimate must be attributed to the beyond-footprint roughness. It shows the echoes from microroughness superimposed on (a) a flat interface (no slope), and (b) a linear profile (with a given slope).

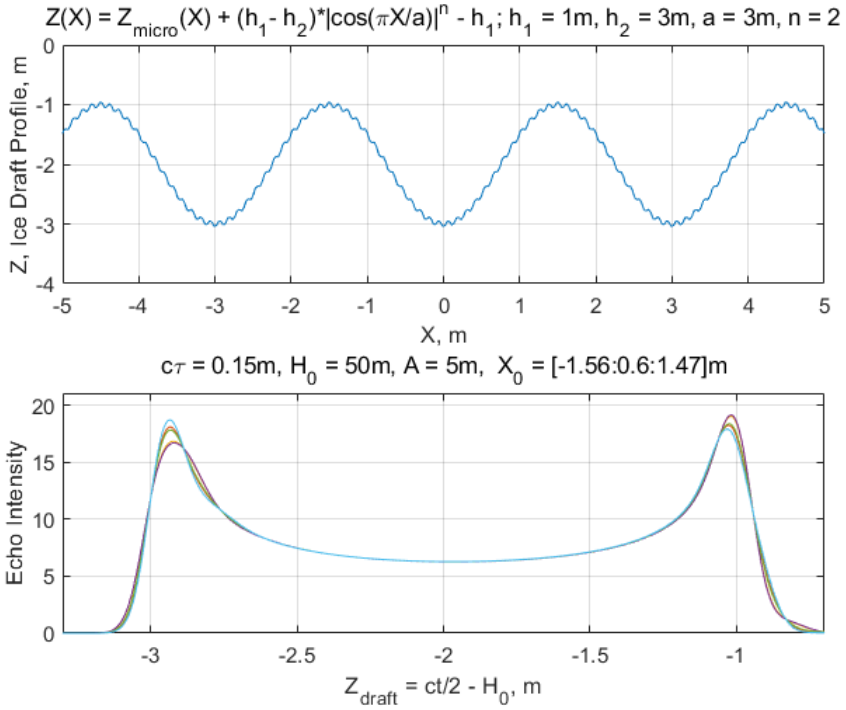

(a)

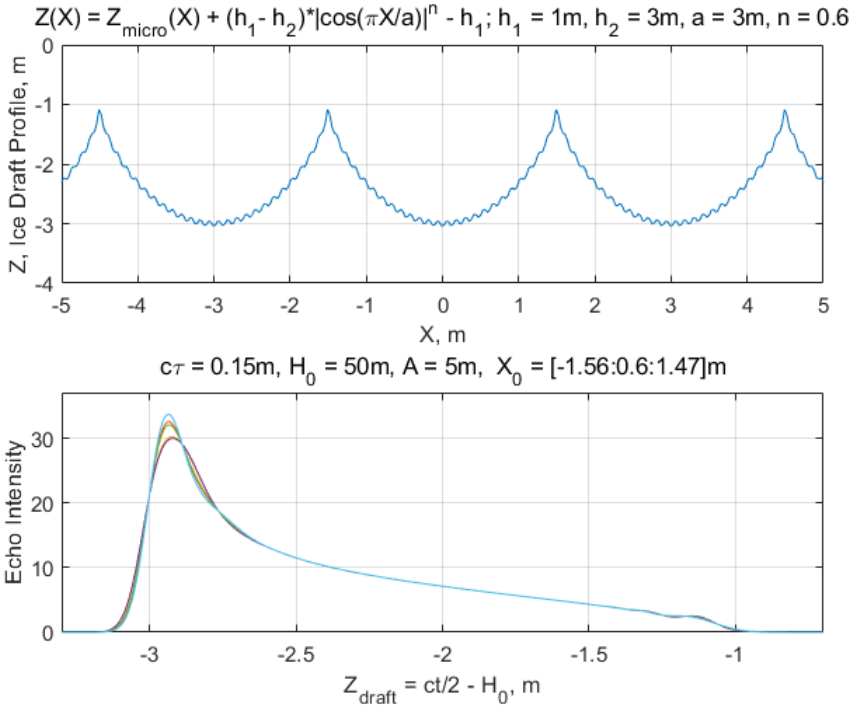

(b)

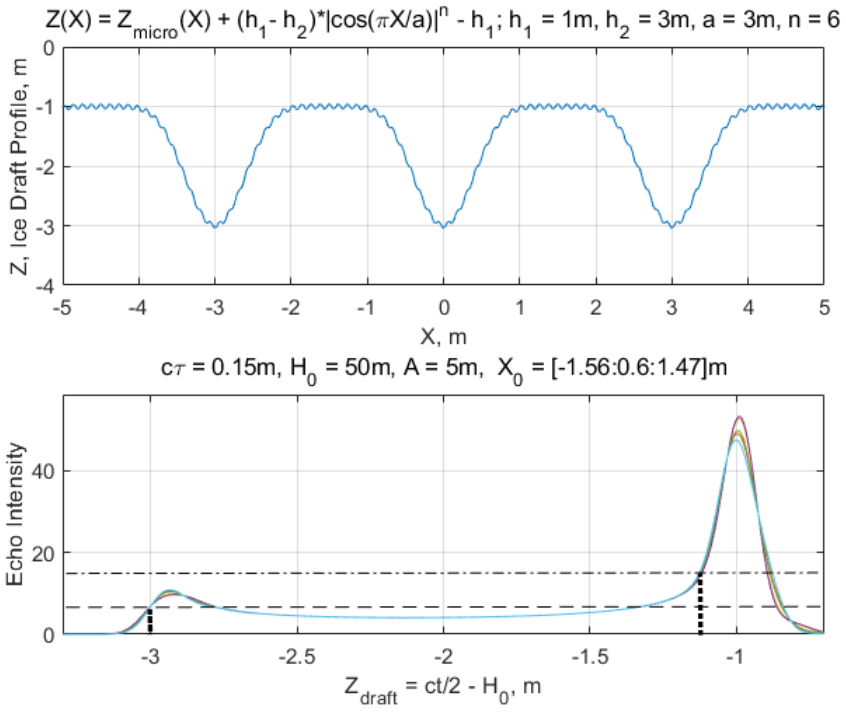

(c)

Figure 2: *Effect of within-footprint macroroughness (upper subplots a, b, c) on the shape of the ULS echo time series (lower subplots) and on the ice draft estimated from the echo leading edge.*

Effects of within-footprint roughness are shown in Fig.2. For simplicity, the macroroughness is 1D and varies within the depths 1 to 3m periodically with the period a = 3m. The shapes of the ice profile are shown in the upper parts of subplots a, b, and c. Fig.2a shows the echo for a sinusoidal macroroughness/profile of ice, 2b – for a profile with flatter crests and sharper troughs, and 2c – for a profile with sharper crests and flatter troughs. The curves of different colors correspond to different horizontal positions of ULS due to moving (relative to the ice canape) with consecutive equidistant shifts within total 3m shift.

These simulations demonstrate that the shape of within-footprint roughness may significantly affect the shape of the echo time series. Some practical conclusions can be derived, which may be important for better understanding ULS data. For instance, comparison of the echo time series in Figs. 2b and 2c shows that estimating the draft from the echo leading edge may significantly depend on the detection threshold and/or the receiver gain: higher threshold or lower gain may result in the estimate corresponding to the second maximum of the intensity time series (see Fig. 2c), whereas lower threshold or higher gain may result in the estimate corresponding to the first maximum.

A more detailed analysis of Eq.1 and simulations result in a simple qualitative estimate for the received echo duration, $\tau_r \approx \tau + \frac{2\Delta h}{c}$, where Δh is the estimate for the within-footprint draft variations. In terms of the scaled time, instant draft, used in Fig.1, this is equivalent to the relation $\Delta Z_{draft} = c\tau_r/2 \approx c\tau/2 + \Delta h$. This relationship shows, for instance, that the within-footprint roughness can be estimated if not only the echo arrival time, but also the echo duration is measured, and, also, that shorter pulses are preferable for improving such

estimates. For instance, if echo, such as any of those in Fig.1, is recorded by ULS, the estimate for within-footprint roughness is ~2m, assuming that the detection threshold can be chosen low enough (limited only by noise level). In addition, if the shape of the measured echo time series is similar to one of shown in Fig.1, the corresponding type of the ice roughness can be suggested.

1.3 ULS data analysis

One of objectives of this research was to examine a data set acquired by Dick Moritz in 2003 using a monostatic 300 kHz ULS system at the APLIS ICEX03 camp and described in detail in his notes [Moritz (2016)]. ULS was deployed through a hydro hole with weights on the tether and data cable to allow the ULS to drift away in the direction of the relative current in the upper ocean. Map of and some details of the ULS deployment are given in **Figure 3**.

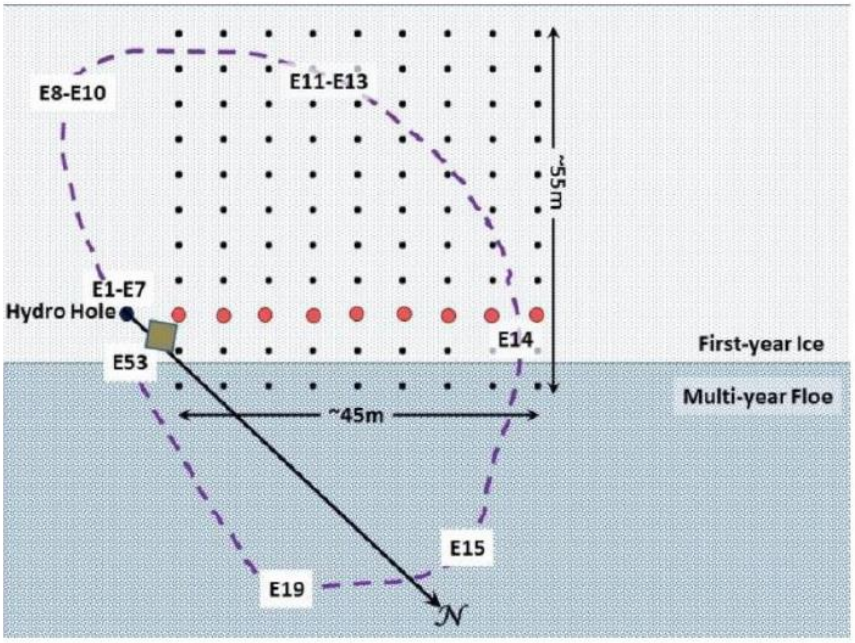

Figure 3: *Map of ULS deployment at APLIS ICEX 2003 (cortesy of R.Moritz). The azimuth and distance from the hydro hole to the ULS are indicated schematically by the dashed purple curve. 53 experiments were performed, E1-E53, each at a fixed depth and location along the curve, with experiment number increasing in the clockwise direction. Ancillary measuremnts of ice draft, ice thickness and snow depth were made at the red dots (auger holes) and at the 9* x *11 grid points (EM 31 and snow probe).*

The measurements were made at different sonar depths (27-67m) under different types of sea ice, nearly flat first-year ice (FFYI), non-flat first-year ice (FYI), deformed multi-year ice (MYI), as well as deformed ice in the transition zone between FYI and MYI types. Each of 53 experiments typically consisted of 36 pulses of rectangular envelope, with transmit pulse duration 1ms (~70 cm for the half-pulse length). Given the ULS depths and half-beam width, $\sim 2.5^{\circ}$, foot-print sizes were 1-3 m. Received voltage time series (echograms) were recorded (1853 pulses in total) and achived along with the ULS depth, see **Figure 4**.

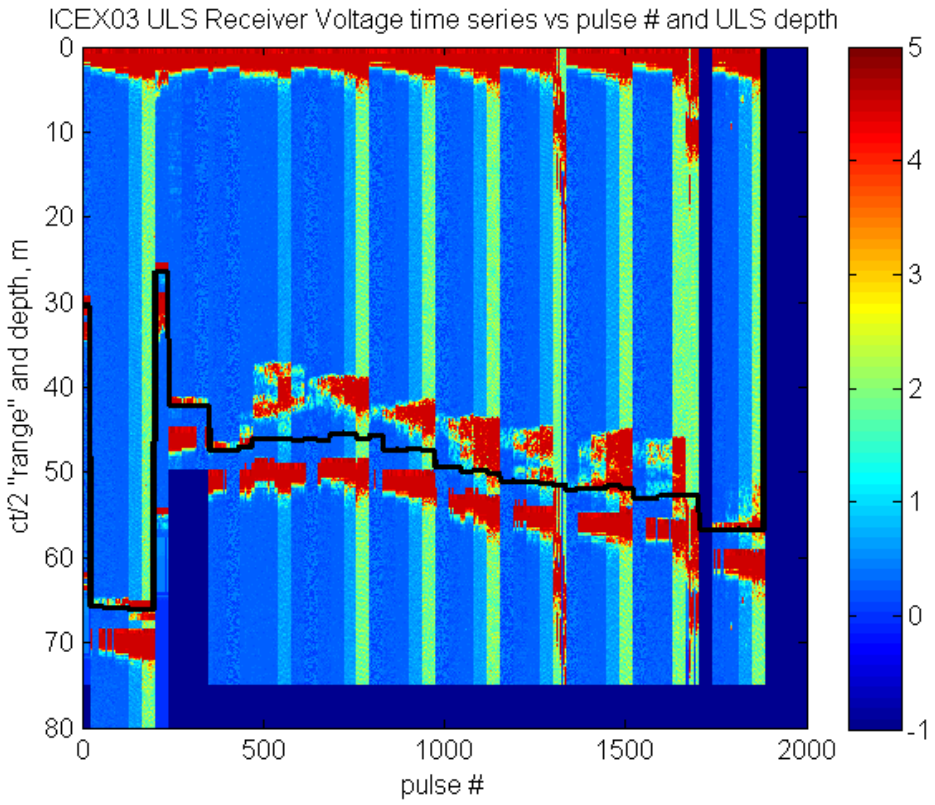

Figure 4: *ULS echogram - ICEX03 backscatter intensity/voltage time (range) series for all 53 experiments and all gains. Black curve shows ULS depth at each experiment.*

An example of a data subset for echograms is given in **Figure 5** that shows 36 echo intensity time series (in log-scale) for experiment #3 made under non-flat first-ear ice (FYI).

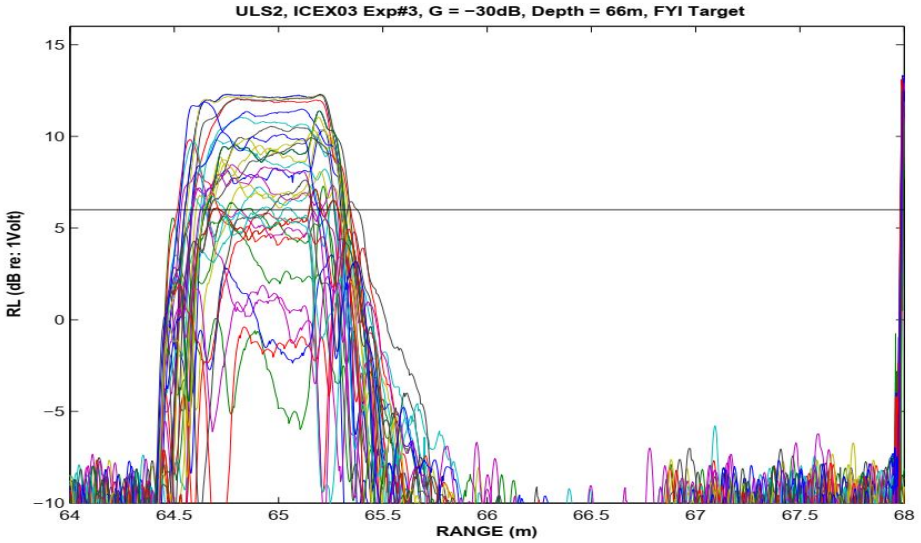

Figure 5: *ICEX03, experiment #3, ULS echograms (voltage envelope time series) for all 36 pulses. "Range" is a scaled time, ct/2. Commercial ice profilers use only time of arrival estimated for the echo leading edge, which depends on the chosen gain (here -30dB) and detection threshold (horizontal line, 2V, shown in log scale).*

Note that normally, to estimate the ice draft, ULS-based profilers use only time of arrival for echo leading edge. Such estimates, however, depend also on chosen detection threshold and gain. In Fig.6, the first crossing of the threshold is used for retrieval of the range/draft (which is not always possible, as some curves' maxima are below the threshold). Another parameter of the echo can be estimated using the range of last crossing, the echo duration. Frequently, higher gains are preferred to provide a better contrast of the received echograms (or making the echo edges steeper).The effect of higher gain is somewhat similar to the effect of reducing the threshold at which the signal arrival time and duration are evaluated. If either lower threshold or higher gain was chosen, the first crossing (leading edge) range would give only a slightly smaller value, while the last crossing range could be significantly larger e.g. in the case of the echo with heavy tail. In a simplest opposite example of a rectangular shape, the gain does not affect the duration at all. Therefore, the relationship between the retrieved echo duration and the receiver gain can be utilized for a parameterization of the echo shape, which, as was discussed earlier, is related to the ice roughness, and possibly to the ice type/edge.

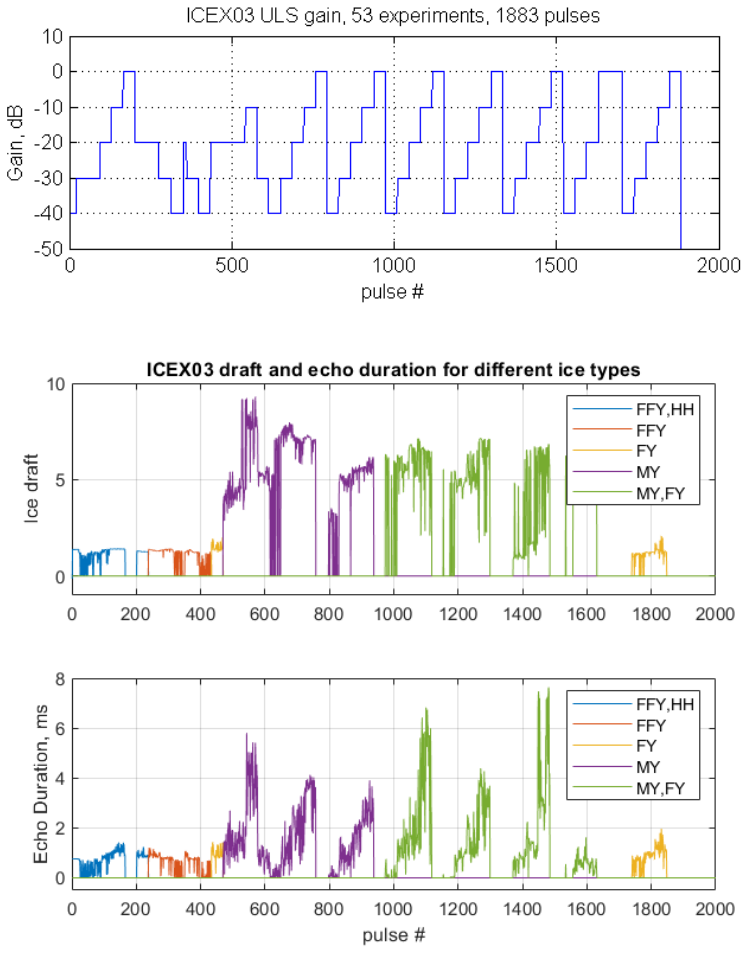

Figure 6: *Receiver gain used in each of 53 experiments (upper panel), Ice draft (center) and echo duration (lower panel) estimated for all 1883 pulses and ice types (shown in different colors). Experiments where the type is not defined are shown in green.*

To illustrate these effects, **Figure 6** (upper panel) shows the ULS receiver gain for all 1883 pulses. In each of 53 experiments the ULS depth and gain were fixed, whereas ULS location relative to ice was slightly varying. The ice draft and echo duration inferred from the echo time series estimated for each of 1883 pulses are presented in Fig.6 (center and lower panels), with the ice type shown as well by different colors.

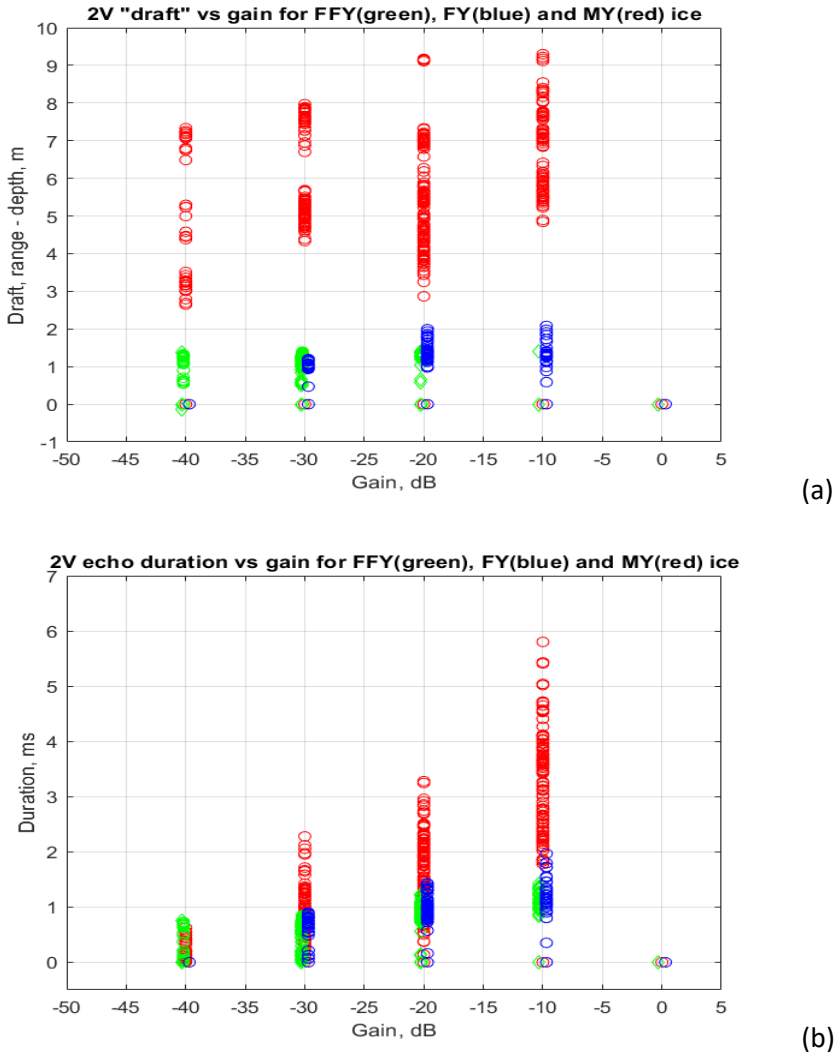

Figure 7: *Ice draft (a) and echo duration (b) estimated from ULS echoes shown vs receiver gain for different ice types, nearly flat first-year ice (FFY, light green), non-flat first-year ice (FY, blue), deformed multi-year ice (MY, red).*

In **Figure 7**, using the same data, the ice type is shown as an output of the draft-gain (a) and duration-gain (b) variables respectively. Fig.7a confirms the known tendency for multi-year ice (shown in red) to be thicker. It also shows a slight increase of the draft estimate with increasing the used gain. In many cases, however, this effect can be considered negligible for both ice types, multi-year and first-year ice. On the contrary, Fig.7b demonstrates a much stronger effect for dependence of the estimated echo duration from the used gain and shows a way to quantify an important (but not used) fact that in the case of multi-year ice the echo shape has a much heavier tail than in the case of first-year ice.

A large enough number of echoes (typically 36) measured at each nearly fixed location made it possible to examine a "local statistics" for the ULS output parameters, the mean and standard deviation for draft and echo duration, derived from the echo time series separately for each experiment. The goal was, having a ULS data set, such as shown in Figs.6 and 7, to see a possible relationship between these "local statistics" and the ice type/age.

The standard deviation, S, was defined as $S = \sqrt{\frac{1}{N-1}\sum_{i=1}^{N}(B_i - D)^2}$, $D = \frac{1}{N}\sum_{i=1}^{N} B_i$, where D is the mean of a random variable vector, **B**, here the draft or echo duration, made up of N scalar observations. Results are shown in six panels of **Figure 8** for each of six pairs made of the four parameters, mean and standard deviation of draft and echo duration.

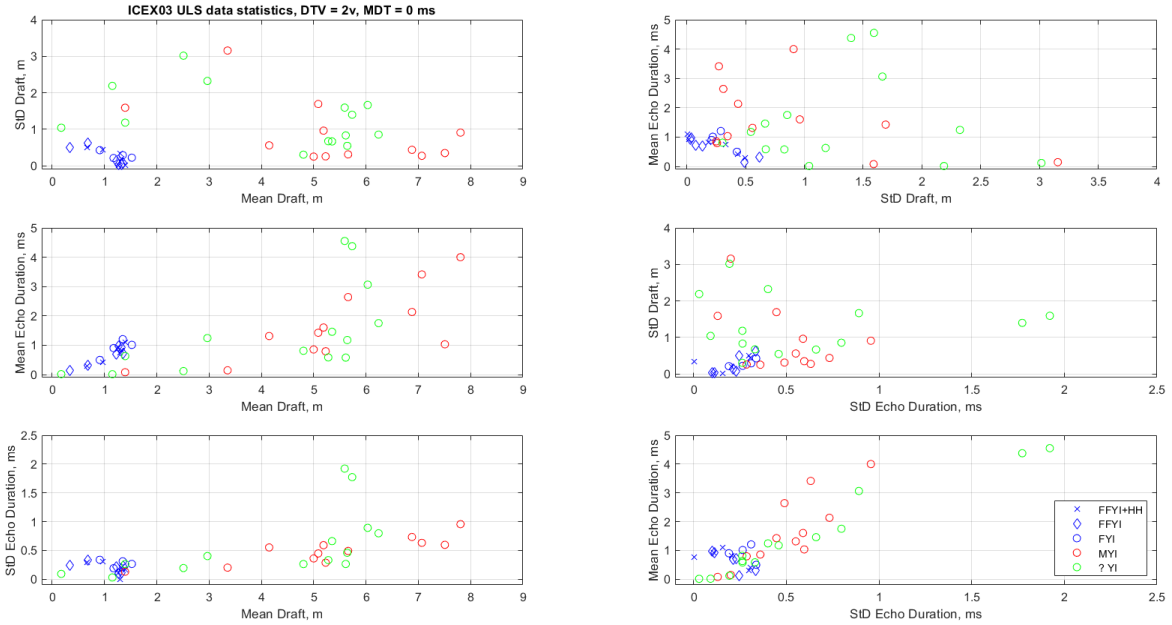

Figure 8: *Statistics of the parameters derived from measured echo time series, mean and standard deviation for draft and echo duration, for all 53 experiments, shown for first-year ice (in blue), multiyear ice (red) and unknown type (green).*

A noticeable general feature is that all these estimated parameters derived from the ULS data, tend to be smaller for first-year ice (shown in blue) than for multiyear ice (red). Also shown are data for locations where the ice type is unknown (in green). A comparison of the three cases allows to suggest an efficient way to predict the ice type given the local statistics of ULS data.

To demonstrate the algorithm, results obtained using only statistics of the ice draft, its mean and standard deviation, are shown separately in **Figure 9**. This case can be particularly important as it is applicable to analysis of common ULS data where only the draft is archived, see, for instance, Schweiger (2016). Consider first only the data where the ice type is known (i.e. shown in blue and red). If only the mean draft D is used, the ice type prediction can be either first-year or multi-year ice, see data for $D<d \approx 2$ m. The same ambiguity is in the case where only standard deviation S is used, see data for draft $S < a \approx 0.7$ m. But if the results are plotted in the 2D space of both variables, S and D, as in Fig.9, than all data obtained in

locations with one of three known first year ice types, shown in blue, are clustered within the ellipse (shown by the dashed curve) where both variables are small enough, so that $\left(\frac{S}{a}\right)^2 + \left(\frac{D}{d}\right)^2 < 1$, while all the multi-year ice data, are beyond this ellipse. If the ellipse criterium is applied now to the data obtained for unknown ice type (shown in green), the prediction would be unambiguous and clear – multi-year ice.

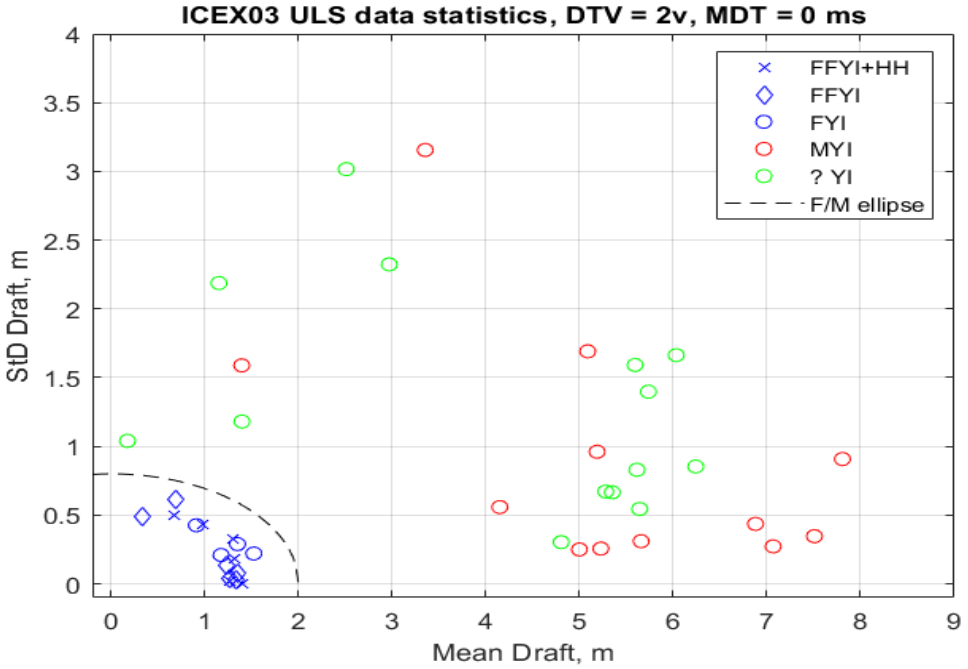

Figure 9: *Relationship of the ice type/age and statistics of parameters derived from measured echo time series, mean and standard deviation of the ice draft, for all 53 experiments. The data for all types of first-year ice, shown in blue, are clustered within the ellipse having semi axis d=2m and a =0.7m (shown by the dashed curve), while the data for multi-year ice (shown in red) – beyond the ellipse. Experiments where the ice type was not known are shown in green (see also the top panel in Fig.8). According to the ellipse criterium, the suggested ice type is the multi-year.*

1.4 Laboratory experiments: effects of ice heterogeneity

In previous sections of this report, most recent results are described that were obtained in 2019 and 2020 and not included to the previous report, Ivakin 2019b. This section, for completeness, gives a description of earlier results obtained under this project and briefly reported in Ivakin 2019b.

In this project, a laboratory study of the effect of heterogeneity on acoustic properties of ice was performed [Ivakin et al, 2018]. The measurements were made on cylindrical laboratory-grown ice samples serving as proxies for two types of sea ice with different microstructure. The ice samples were prepared by B. Light, APL-UW. The first one, congelation ice, had relatively homogeneous structure typical of first-year sea ice. The second one, granular ice, with a more heterogeneous microstructure, was prepared as a proxy for retextured multiyear sea ice. Both samples had approximately equal bulk salinity (12 ppt) to isolate effects of different microstructure.

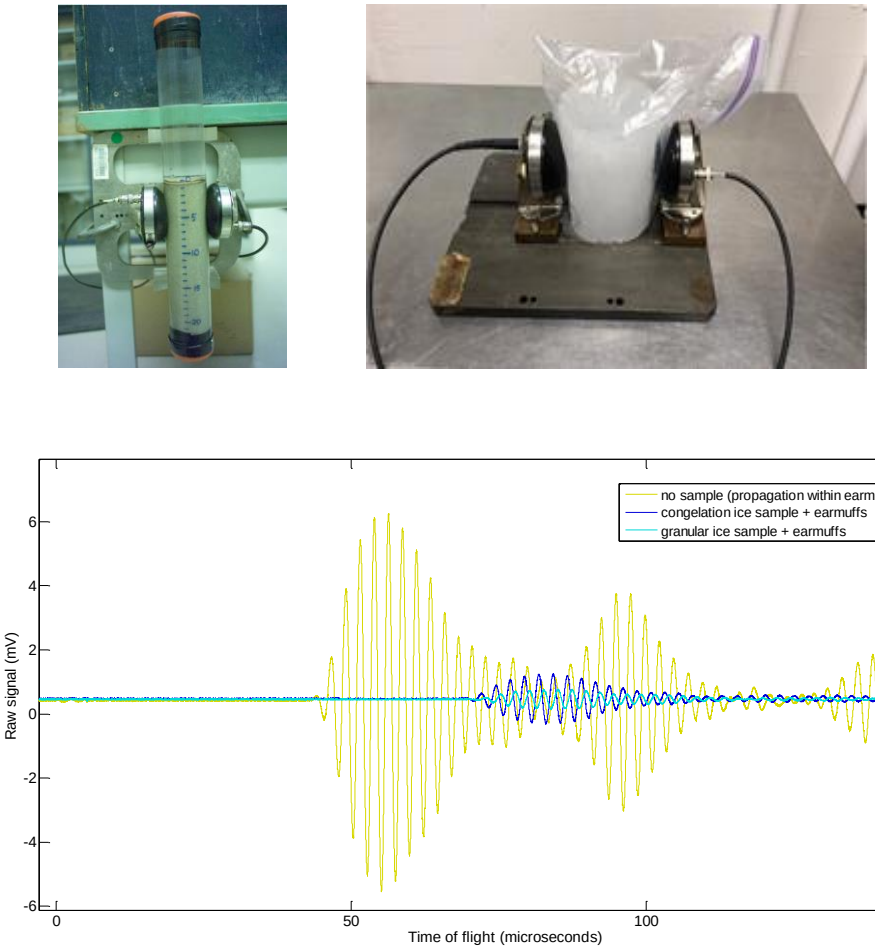

Figure 10: *The "earmuff" transducers used with sediment (upper left) and ice (upper right) core samples, and Voltage time series (lower panel) measured on the two ice core samples compared to the no-ice case.*

The ice samples were used for acoustic measurements performed using the "earmuff" transducers borrowed from NRL SSC where they were used previously for sensing sediment cores, **Figure 10** (upper panel). Speed and attenuation in ice were estimated by measuring time of flight and magnitude of 400 kHz pulses. In Fig.10 (lower panel), Voltage in received signals as function of time is shown for three cases: (1) no ice (internal earmuffs propagation, shown in yellow), (2) congelation ice sample (shown in purple), and (3) granular ice sample (shown in green). The granular (very inhomogeneous) ice sample showed a lower speed and enhanced attenuation of the acoustic signal relative to the congelation (relatively homogeneous) ice case. Sound speed was found in granular ice to be about 5-10% lower and more varying (spatially) than in congelation ice. Error bounds were estimated to be within 1% based on the same measurements made for plastic material with known sound speed. Also, the granular ice sample showed enhanced attenuation of the acoustic signal relative to the congelation ice case. The results confirm sensitivity of sound speed in ice to its internal microstructure and heterogeneity. This motivates further research with a goal to develop an acoustic sensing technique for sea-ice characterization and, in particular, discrimination between relatively homogeneous first-year ice and multiyear (heterogeneous) ice types.

1.5 Suggestions for follow-up research

In a recent ONR-AG planning letter, Ivakin (2020), we proposed a follow-up research to develop a technique for estimating sea-ice physical and mechanical properties and their depth-dependence within the ice layer based on direct through-ice-core measurements of sound speed and attenuation. Based on this technique, we can develop a portable system to be used in both laboratory and field conditions. The system is suggested to be calibrated in the lab using a variety of samples with known (and measured by other established methods) properties. As such, we would exploit a set of homogeneous plastic samples already used in our preliminary experiments. Some porous water-saturated materials with microbubble inclusions would be used as well to test the system response and sensitivity to the ice heterogeneity (to confirm and extend results obtained under this project). Final tests would be carried out using cores of natural ice.

Another potential follow-up research could exploit the results of ULS data analysis presented in previous sections of this report. Particularly, the ellipse criterium may be used as a simple quantitative algorithm for distinguishing first-year ice from multi-year ice and applied to other data available in the ice draft and ULS archives (such as BGEP and CANAPE datasets), as well as be used in future experiments.

1.6 References

Frantz A.M., B. Light, S.M. Farley, S. Carpenter, R. Lieblappen, Z. Courville, M.V. Orellana, and K. Junge (2019), "Physical and optical characteristics of heavily melted "rotten" Arctic sea ice", *The Cryosphere*, **13**, 775-793.

Ivakin A.N. (1998), A unified approach to volume and roughness scattering. *J. Acoust. Soc. Am.*, 103(2), 827-837.

Ivakin A.N., W. Kreider, and B. Light (2018), "Measurements of sound speed in two types of ice with different microstructure", *J. Acoust. Soc. Amer.*, **144**(3), Pt.2, p.1819 (A); doi:10.1121/1.5068025

Ivakin A.N. (2019), "A time-domain model of high-frequency backscatter from sea ice with applications to upward looking sonar data analysis", *J. Acoust. Soc. Amer.*, **146**, 3029 (2019).

Ivakin A.N. (2019b), ONR yearly report, Award Number: N00014-17-1-2196, 15 June 2019.

Ivakin A.N. (2020), Sea-Ice Characterization Based on Direct Through-Core Measurements of Ultrasound Speed and Attenuation, ONR 322AG Core Planning Letter, submitted in Oct 2020.

Jackson D.R., Odom R.I., Boyd M.L., Ivakin A.N. (2010), A geoacoustic bottom interaction model (GABIM). *IEEE J. Ocean. Eng.*, 2010**,** 35(3), 603-617.

Jackson D.R. and M. D. Richardson (2007), High-Frequency Seafloor Acoustics (Springer, New York), Appendix G, pp. 493–508.

Moritz R.E. and A.N. Ivakin (2012), Retrieving sea-ice thickness from ULS echoes: Methods and data analysis. *Proc. Inst. Acoustics*, v.34: Part 3 *(ECUA2012)*, pp.1535-1542.

Moritz R.E. (2016), ICEX03 ULS Voltage Dataset, 29 October 2016.

Schweiger A.J. (2016), Unified Sea Ice Thickness Climate Data Record, Polar Science Center, Applied Physics Lab., Univ. of Washington, *psc.apl.washington.edu/sea_ice_cdr* , digital media.

Weeks W.F., and S.F. Ackley (1986), "The growth, structure, and properties of sea ice", in *Geophysics of Sea Ice*, N. Untersteiner (Ed.), Plenum Press, NY, pp.9-164.

2 MF propagation and reverberation under sea ice: Modeling and data analysis

2.1 Summary

This part of the project is aimed on developing a physics-based modeling approach to acoustic propagation, scattering, and reverberation in the Arctic ocean. The approach will help to better understand mechanisms which control low- and mid-frequency propagation and reverberation under sea ice that will allow quantitative interpretation of existing data and develop a necessary theoretical base for optimal planning experiments in the Arctic. A long-term goal is to improve prediction of propagation and reverberation under ice and to provide a wide-area synoptic assessment of ice properties, particularly spatial ice type distribution in complicated arctic environments. This project suggests a modeling approach which accounts for waveguide propagation effects and multiple interactions with rough ocean boundaries.

One of specific objectives of this research includes analysis of a dataset obtained during ICEX14 in a deep (3 km) ice-covered ocean environment using a MF source of opportunity located at a 719 m range from the receiving system, ALAS. Both source and receiver were located at ~30m depth. The dataset includes time series of acoustic intensity received from five consecutive 5s-long 3.5 kHz CW pulse transmissions, one per minute. The time series showed a clear direct arrival (blast signal) followed by an about 30s-long reverberation coda.

A model is developed that considers under-ice waveguide propagation and includes multiple reflections and scattering from the ocean bottom and ice canopy. The model shows that the direct signal, corresponding to nearly horizontal propagation, is strongly affected by presence of a weak near-surface (within 50m depths) acoustic channel. Bottom- and ice-bounced arrivals from steep angles are controlled by reflectivity and scattering strengths of ice and bottom, their physical properties and acoustical parameters, particularly the bottom sediment layer and ice layer thicknesses. Some other effects that may be caused by variability of the sound speed profile and absorption in water, as well as effects of system parameters (e.g., the source/receiver depths, used pulse length, etc.) are considered. Possibilities of inversions for water column, bottom and ice parameters based on analysis of this and similar experimental datasets are examined.

2.2 ICEX14 ALAS dataset

The dataset was obtained during ICEX14 in a deep (~3 km) ice-covered ocean environment using a MF source of opportunity and a receiver of Arctic Line Arrays System (ALAS) developed as part of a DARPA funded effort, described by Williams et al in Ref.[1]. The receiver and source were omnidirectional, located under ice at 30 m depth at a ~719 m range from each other [2]. Five consecutive 5s-long CW pulses @3.5 kHz were transmitted, one per a minute. **Figure 11**, left, shows transmission loss, i.e. relative intensity (squared magnitude of received pressure envelope per unit source level) for all five timeseries (in blue) and average over the five pings (in red). The data represent distinctly different behavior in two different time intervals. The short-time interval (~ 0.5 — 5.5 s) corresponds to direct arrival of the 5s-long pulses transmitted from the rather short direct-path distance (719 m).

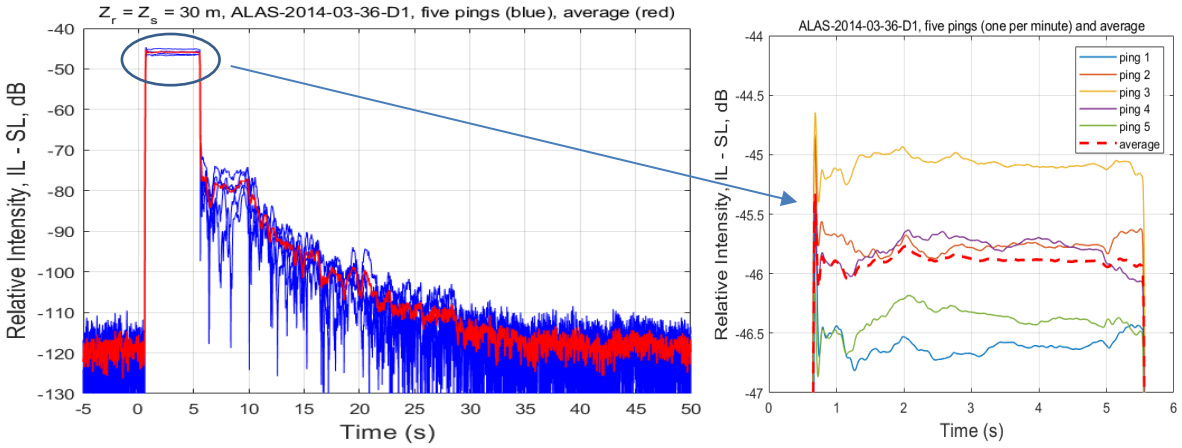

Figure 11: *ICEX14 Transmission Loss time series measured by ALAS system; left — the entire unaveraged (blue) and average (red) TL time series; right — zoomed-in direct arrivals (blast signals) shown for all five time series (pings 1-5, different colors) and for their average (dashed red). This gives for the measured transmission loss of the direct arrival signals an estimate TL≈-45.9±0.9dB.*

The TL time series, zoomed-in in the right panel of Fig.11 for detail, is within approximately 1dB variations around the average value of -45.9dB. The direct arrival signal is followed by a reverberation coda (left panel) whose time interval above noise level is t ~ 5.5 — 35 s, which corresponds to medium ranges, $ct/2$ ~ 4 — 25 km. Note that the reverberation signal actually starts at ~ 4 s that corresponds to the 3 km range (the bottom depth), although it can be seen only after ~5.5s time because its beginning (at ~ 4 — 5.5 s) is well below the level of direct blast signal. Also note that the source and receiver clocks were not synchronized, so the estimates for direct arrival time and related parameters assume a typical sound speed in the water under ice, c = 1460 m/s.

2.3 Transmission loss: The short-time interval

As a reference for an initial comparison, TL due to the spherical spread for the direct path can be taken, which at the 719m range gives an estimate ~ -57dB, i.e. the measured TL is about 11 dB greater (~ -46 dB). Most of the difference can be explained the effect of surface-duct, a typical feature of the Arctic environment. For rough estimates, consider a simplified version of sound speed profile (SSP) for a surface duct schematically shown in **Figure 12** (left) and a corresponding scheme of multi-path propagation, Fig.12 (center and right).

A simple ray-based consideration and a combined (coherent and incoherent) summation of intensities (see comments to Fig.12) gives an enhancement factor of up-to 8 compared to a reference intensity (-57 dB) and, with adding 9 dB, result in TL_{ray} ≈ -48 dB. In more accurate estimates, the factor can be smaller due to reflection loss at the ice-water interface and to "slightly" different spreads along incoherent paths ("slightly" because the difference is not as big as exaggeratedly shown in this figure, for all paths are nearly horizontal). However, this reduction can be well compensated by possible focusing effects of refraction, which can e.g. result in a caustic near receiver. Note also that the propagation scheme shown in Fig.12 corresponds to a "medium-range refraction" scenario where only one group of four refracted paths appear. The long-range scenarios with multiple 4-path groups are not considered here.

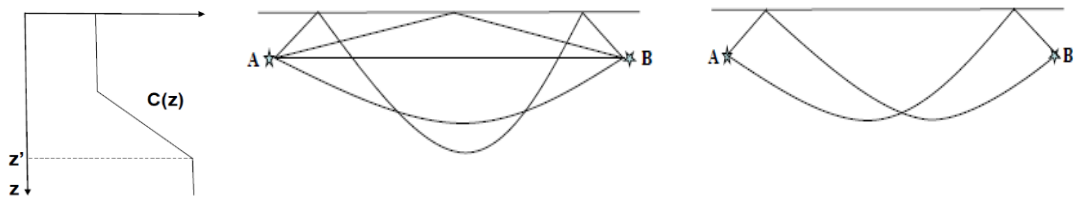

Figure 12: *A scheme of propagation in a surface duct under ice considering a simplified sound speed profile (left) that allows a certain number of paths (center and right). Two of them, the direct one (shown by a horizontal line between source A and receiver B) and that with one bounce from ice (center), appear even at very small ranges and if there is no duct. The other two paths shown in the center and two in the right panel, are caused by refraction, have turning points within the gradient layer (above z'), and do not appear if ranges are too small. The two in the right are in-phase "coherent" paths, while the four in the center are out-of-phase "incoherent" paths.*

More accurate (than ray-based) calculations of TL can be made using full-wave codes, such as PE-based ones, if SSP is known with sufficient accuracy. **Figure 13** (left) shows an average depth-dependence of sound speed measured during the experiment in the ICEX14 area [2]. It represents a rather typical for the Arctic environment near-surface duct within first 50m depths. While it's relatively weak (with only ~ 7 m/s variations of the sound speed within the duct), it happened to be sufficient, even at such short ranges, to cause a "caustic-like structure" near the receiver location. This can be seen in Fig.13 (right), which shows 2D (range-depth) contours for full-wave intensity (TL) calculated at relevant here ranges and depths using this SSP.

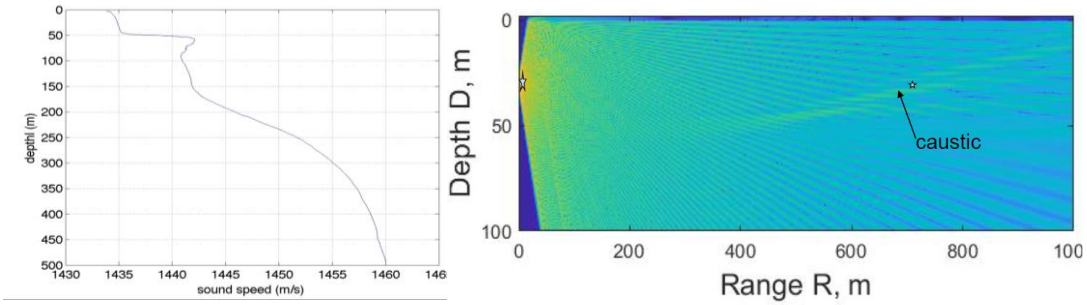

Figure 13: *An average sound speed depth-profile in the ICEX14 area (left) and a range-depth image of full-wave intensity (right), corresponding to this environment and a short range, 719 m, between source and receiver (shown by stars). Note a "caustic-like structure" near the receiver location caused by focusing effects of refraction in the surface duct (within 50 m depths).*

The intensity (TL) was evaluated using PE (parabolic equation) simulations given the source depth and ice layer thickness (2m) typical for the area [1]. The results are shown in **Figure 14** for TL as a function of range at slightly different receiver depths (upper panel) and for TL as a function of depth at slightly different receiver ranges (lower panel). All the curves, as expected, are strongly oscillating and give TL values very sensitive to the receiver location (and the source location as well, due to the reciprocity principle). Assume, for instance, that source/receiver exact locations allow some uncertainty around nominal values, say $\pm$1m

vertically and ± a few m horizontally, which for the source of opportunity in this experiment is a reasonable conjecture. Then averaging of calculations within that uncertainty gives rough bounds for a PE-based transmission loss estimate with corresponding uncertainty bounds, $TL_{PE} \approx -48 \pm 2$ dB, that is about the same as the made earlier rough ray-based estimate.

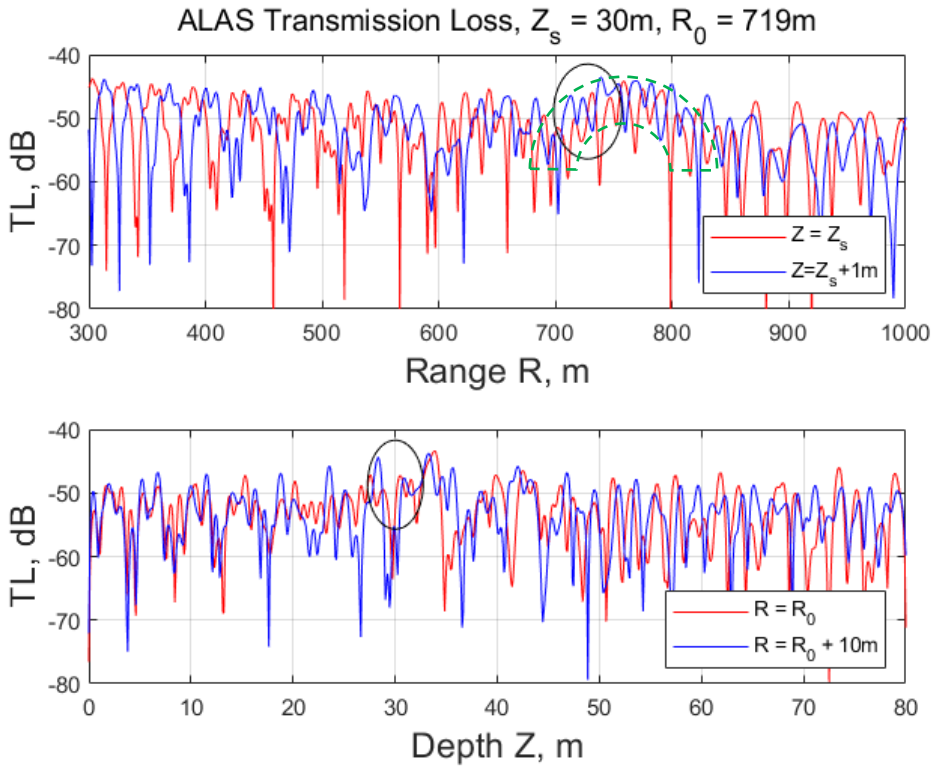

Figure 14: *Transmission Loss (TL) derived using PE simulations of propagation in the under-ice waveguide with SSP shown in Fig.15. TL is given as a function of range at slightly different receiver depths (upper panel) and as a function of depth at slightly different receiver ranges (lower panel). Averaging TL oscillations within some bounds (shown by ovals) due to somewhat uncertain geometry and SSP parameters provides rough bounds for a PE-based estimate of transmission loss with corresponding uncertainty bounds, $TL_{PE} \approx -48 \pm 2$ dB. A green dashed semi annulus (in upper panel) envelopes an enhancement area with TL oscillations that correspond to a "caustic-like structure" near the receiver location mentioned in Fig.13.*

Although both estimates, ray- and PE-based, are within a reasonably good fit to rough bounds of measured transmission loss, $TL \approx -46 \pm 1$dB (see Fig.11), the difference (~2 dB) can still be informative. For instance, it can be caused by SSP evolution within the 5 min time span that includes all the five pings. More accurate predictions for TL, however, would likely require more detailed dynamic SSP inputs, e.g. modeled or measured, with sampling once per minute along the direct arrival path. For instance, as it was mentioned earlier (see comments to Fig.12), this would accurately determine those paths which have turning points within a thin gradient layer (at about 50 m depth for the SSP shown in Fig.13). Even small variations of this layer depth, e.g. caused by internal waves, may change the number and intensity of refracted paths at this small range (719 m), compensate the ~2dB difference, and possibly provide a way to acoustically monitor dynamics of the gradient layer.

2.4 Medium-range reverberation: Bottom and ice reflection and scattering

Note that the PE model, used here to describe the direct arrival, is a small-angle approximation of the full-wave solution, i.e. it includes automatically all possible nearly horizontal short-range paths with ice reflections and in-water refractions, but excludes nearly vertical bottom and ice reflections which arrive later along medium-range paths as a part of reverberation coda. These steep-angle paths are practically not affected by water stratification, and associated arrivals' intensities can be estimated using an approach close used in [3] and a semi-coherent Multiple Specular Reflections (MSR) model described there. The approach here is modified for adjustment to an ice-covered medium-range deep-ocean scenario, whose typical details are described, e.g., in [4].

One such modification is that the model includes now the case of non-free water surface which is given by a frequency-angular dependence of the ice reflection coefficient. Another modification exploits conditions, rather common for deep water scenarios, that source and receiver depths are much smaller than the ocean depth. This allows a simplified treatment of the so-called "4-paths semi-coherent effect" in terms of an "effective directivity" of source and receiver placed on the water-ice interface whose reaction is defined by reflection coefficients of ice at outgoing (from the source) and arriving (to the receiver) angles from nadir. In general, this similar to introducing the "effective directivity" in Eq.1. Then the "4-paths effect" is automatically included for all propagation paths between ice and bottom. Also, the two-way propagation loss factor $P(r)$, see Eq.2, is corrected to account for additional loss due to multiple reflections along these paths. Consider first the case where the ocean boundaries are flat. In this case, all the paths that include only specular reflections at the bottom and ice. The result is given in **Figure 15**.

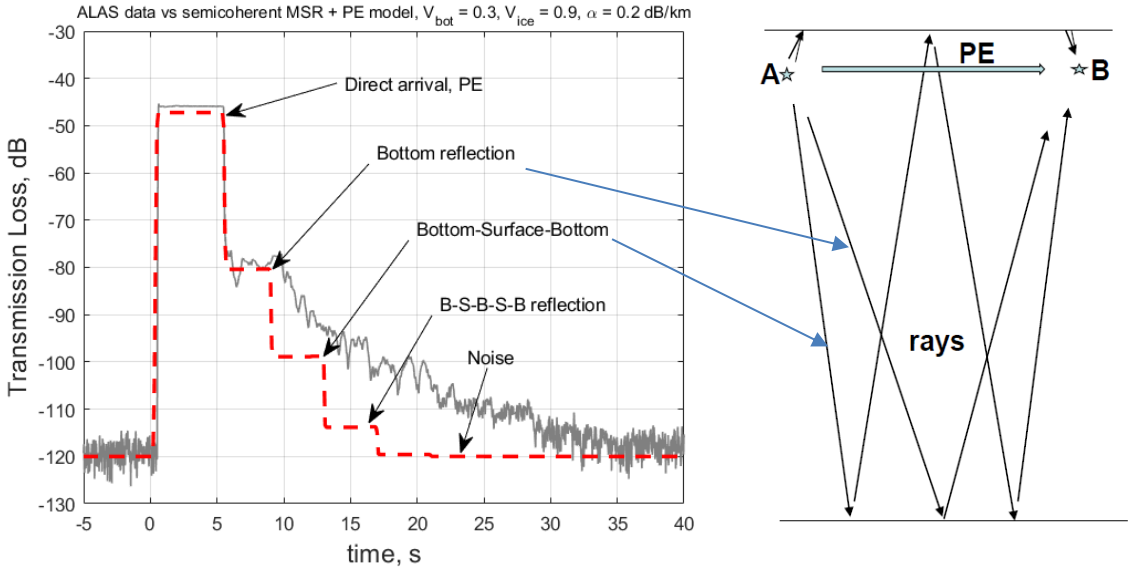

Figure 15: *ALAS data-model comparison (left) that includes, in addition to direct arrival, only specular reflections from bottom and ice given their reflection coefficients at steep (near normal) incidence, with associated paths (right). For simplicity, the PE arrow here replaces short-range rays and full-wave and rays shown earlier in Fig.12 (center).*

Shown are the model-data comparison for the transmission loss (left) and associated propagation paths (right). ALAS data are used to determine the bottom reflection coefficient V_b, with the ice reflectivity being roughly known (typically, $V_{ice} \approx 0.9$). Then a simple model-data adjustment at the beginning of reverberation signal, in the time interval 6-9 s, requires bottom reflectivity be rather small, $V_b \approx 0.3$. The comparison in Fig.15 shows, however, that the model considering flat boundaries that accounts only for specular reflections from bottom and ice at near normal incidence cannot remove a significant discrepancy appeared at later times. This suggests importance of non-specular scattering from bottom or/and ice and arrivals at non-steep angles and requires examining angular dependencies of reflection and scattering coefficients for bottom and ice. Also, including acoustic absorption in water column can be important for slant paths and correspondingly longer ranges.

The reflection coefficients are specified for two models, an ice layer between water and air (left) and a bottom mud layer over a sand basement (right), shown in **Figure 16** as functions of the incidence angle at different layer thicknesses and a fixed frequency, 3.5 kHz. For simplicity, the ice and bottom poroelasticity were accounted by assuming that their effective densities are slightly complex, see e.g. [11]. Fig.16, left, shows a noticeable sensitivity to ice layer thickness, but only in a limited range of angles, ~ *10º ÷ 25º*. At smaller angles $|V| \approx 0.9$, while at slant incidence angles greater than 25º, the reflectivity is nearly perfect, $|V| \approx 0.98$.

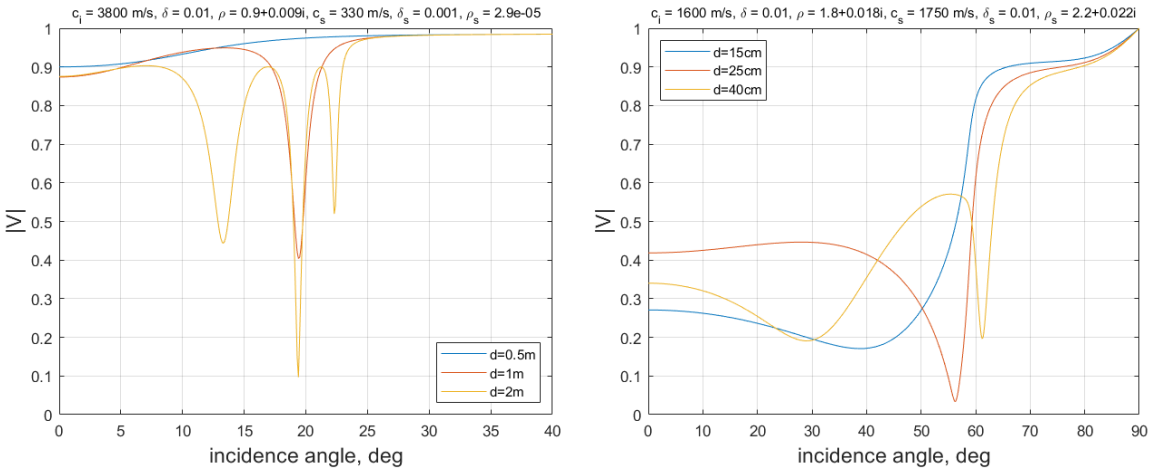

Figure 16: *The reflection coefficients for the ice layer between water and air (left) and the bottom mud layer over a sand basement (right) shown as functions of the incidence angle for different layer thicknesses.*

Of significant importance appears to be including a relatively thin mud layer. As will be shown, both small bottom reflectivity near nadir and much higher reflectivity at slant angles are needed in following model-data comparison. For instance, a model with the 15 cm mud layer over sand half-space provides $|V| = 0.27$ at nadir and $|V|=0.9 \div 1.0$ at slant angles greater than the sand critical angle ~65º, which is impossible for the model without this layer.

In the case of non-flat boundaries, a single scattering approximation is used, i.e. arrivals along paths which include only one non-specular scattering from bottom or ice are included while all others are neglected. In **Figure 17**, two of such arrivals, earliest and strongest ones, are shown (right), and model-data comparison is presented (left).

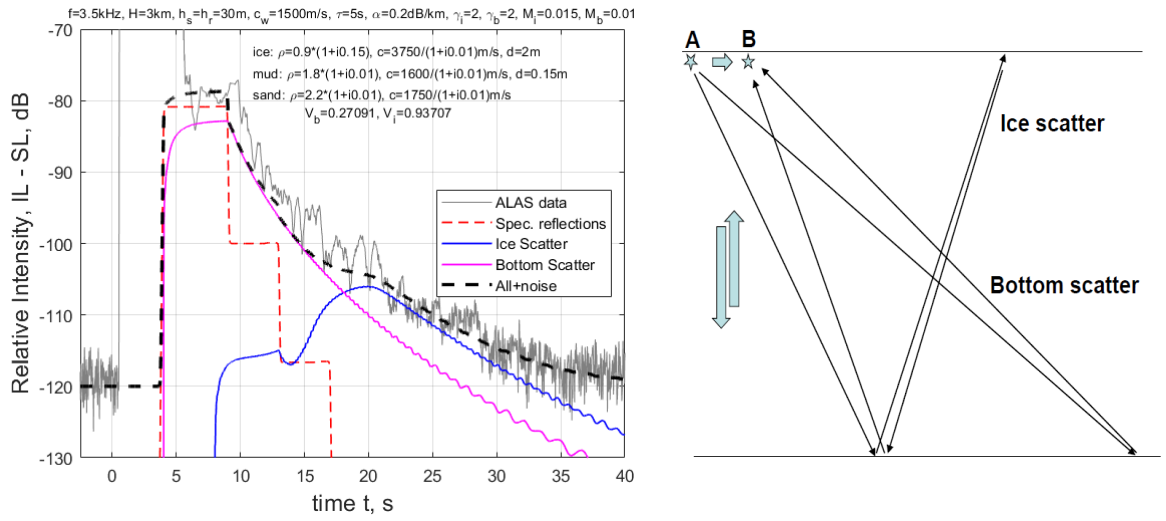

Figure 17: *ALAS reverberation data-model comparison (left) that includes specular reflection and backscattering arrivals from bottom and ice along associated paths (right). Thick horizontal and vertical arrows (right panel) replace multipath components shown in Figs. 12 and 15.*

Model simulations were performed taking into account acoustic absorption coefficient in water, 0.2 dB/km @ 3.5 kHz. Backscattering coefficients for bottom and ice are taken of the same form $m_S(\theta) = M\ (\cos\theta)^{\gamma}$ as in the first part of the report, see Eq.3, assuming unknown strengths M and power exponents γ. These and other bottom and ice model parameters, such as their complex sound speeds, densities, and layer thicknesses, were estimated from model-data comparison (shown in Fig.17, left) and given in Tables 1 and 2.

Table 1: Acoustic parameters of the ice-water-mud-sand layers

	Density, g/sm^3	Sound Speed, m/s	Thickness, m
Ice	0.9 (1 + i0.01)	3750 / (1 + i0.01)	2.0
Water	1	1500	3000
Mud	1.8 (1 + i0.01)	1600 / (1 + i0.01)	0.15
Sand	2.2 (1 + i0.01)	1750 / (1 + i0.01)	∞

Table 2: Parameters of Scattering Coefficient in Eq.3

	Scattering strength, M	Power exponent, γ
Ice	0.015	2.0
Bottom	0.01	2.0

An important conclusion is that all considered mechanisms of mid-frequency propagation and reverberation a deep ice-covered ocean should be taken into account for consistent model-data comparison, each dominating within its own time interval:

- The direct arrival, a multipath signal at short times (0 ÷ 5 s), is strongly affected by structure and dynamics of a surface duct, reflections from ice, refraction in water, and their interference;
- Reverberation signal in the beginning (6 ÷ 9 s) is strongly affected by first bottom reflection, at intermediate times (9 ÷ 17 s) — by backscatter from bottom, and at the end of the coda (17 ÷ 35 s) — by backscatter from ice.

2.5 Other results under the project and suggestions for follow-up research

In previous sections of this report, most recent results are described that were obtained in 2019 and 2020 and not included to the previous report, [5]. This section, for completeness, gives a brief description of earlier results obtained under this project and reported in [5].

A theoretical approach developed in [6] was modified to allow initial estimates of mid-frequency long-range under-ice reverberation. A simplified model of sea-ice layer was suggested to partially include effects of ice elasticity and thickness. The model treats sea-ice as a stratified medium including a very thin water-saturated fluid-to-elastic transitional layer, i.e. ignores elastic properties of the ice just near the water-ice interface. In this case, the effects of ignoring the ice elasticity within the thin transition layer are expected to be insignificant on both the interface contrast parameter defined in [6] and on the propagator factor defined by transmission loss due to propagation within the whole elastic ice layer. Therefore, estimating the intensity of reverberation caused by the water-ice interface roughness, assumed to be small (compared to the acoustic wavelength at mid frequencies), can be made with a sufficient accuracy.

The above-mentioned simplified model of sea-ice has been incorporated in the approach developed in [6], modified and combined with an elastic PE code [7] for the propagator. This allowed developing a new extremely fast code for numerical simulations of the average reverberation intensity in an ice-covered ocean environment [8]. The main goal was to obtain estimates of the influence of ice thickness and elasticity on long-range narrow-band reverberation in a representative Arctic upward-refracting waveguide. The results have been obtained in collaboration with Dr. Scott Frank and presented in [8-10] showing that the effects can be significant, and therefore should be taken into account in further modifications of the under-ice reverberation models and codes.

This research assumes model-data comparisons for reverberation in time domain. A current version of the full-field perturbation approach [12] considers reverberation as a function of range at given frequency. In [13], a modified model is presented that extends the approach to time domain using basic properties of the radiated energy time-frequency distribution (ambiguity function) and the frequency-range interference waveguide invariant. As a result, extremely fast estimations of MF shallow-water reverberation time series were demonstrated which require calculations of Green’s function of the reference medium in the vicinity of the interfaces at only one (central) frequency [13,14].

It was suggested that further work on the technical approach would include development of a time-domain model for long-range propagation and reverberation in deep Arctic ocean [15]. This work would be based on results obtained in this project and would contribute to a theoretical modeling component of the Arctic acoustic research including low- and mid-frequency propagation and reverberation in ice-covered waveguides, particularly for application in CANAPE data analysis [15,16].

2.6 References

[1] Williams K.L., M.L. Boyd, A.G. Soloway, E.I. Thorsos, S.G. Kargl, and R.I. Odom (2018), Noise Background Levels and Noise Event Tracking/Characterization under the Arctic Ice Pack: Experiment, Data Analysis and Modeling, *IEEE J. Ocean. Eng.*, **43**, 145-159.

[2] Williams K.L. (2016), personal communication.

[3] Ainslie M., D. Ellis, and C. Harrison (2016), Low frequency bottom reverberation in a Pekeris waveguide with Lambert rule, *J. Comput. Acoust.*, **24**(2), 1650001-(1-35).

[4] Yang T.C. and T.J. Hayward (1993). III: Measurements of ice and bottom backscattering strengths from medium-range bottom-bounce returns, *J. Acoust. Soc. Amer.*, **94**(2), 1003-1014.

[5] Ivakin A.N. (2019), ONR yearly report, Award Number: N00014-17-1-2196, 15 June 2019.

[6] Ivakin A.N. (2016), A full-field perturbation approach to scattering and reverberation in range-dependent environments with rough interfaces, *J. Acoust. Soc. Am.*, **140**(1), 657-665.

[7] Collis J.M., S.D. Frank, A.M. Metzler, and K.S. Preston (2016), Elastic parabolic equation and normal mode solutions for seismo-acoustic propagation in underwater environments with ice covers. *J. Acoust. Soc. Am.*, **139**, 2672-2682.

[8] Frank S.D., and A.N. Ivakin (2017), Estimating the influence of ice thickness and elasticity on long-range narrow-band reverberation in an Arctic environment, in, POMA: *Proceedings of Meetings on Acoustics*, **30**(1), 070003 (2017).

[9] Frank S.D., and A.N. Ivakin (2018), Long-range reverberation in an Arctic environment: Effects of ice thickness and elasticity, *J. Acoust. Soc. Amer. Express Letters*, **143**(3), EL167-EL173.

[10] Frank S.D. Frank, and A.N. Ivakin (2019), Low-frequency reverberation estimates based on elastic parabolic equation solutions for free-surface and ice-covered Arctic environments, in, POMA: *Proceedings of Meetings on Acoustics*, **35**, 005003.

[11] Ivakin A.N. (2017), A full-field scattering coefficient for rough interfaces and a modified sonar equation for long-range reverberation, *J. Acoust. Soc. Amer.*, **142**(4), Pt.2, 2558.

[12] Ivakin A.N. (2018), A full-field time-domain model for reverberation in complex environments and waveguides with rough interfaces, *J. Acoust. Soc. Amer.*, **144**(3), Pt.2, 1735.

[13] Ivakin A.N. (2018), Backscattering and long-range reverberation in shallow water, in, *Ocean Acoustics*, Proc. L.M. Brekhovskikh's conference, Shirshov Inst. of Oceanology, Moscow: GEOS, pp.114-120.

[14] Ivakin A.N. (2020), Acoustic propagation and reverberation in the Arctic: Modeling, data analysis, and application to remote sensing of sea ice, Planning Letter to ONR-OA, submitted Sept.2020.

[15] Worcester P.F., M.A. Dzieciuch, and H. Sagen (2020), Ocean Acoustics in the Rapidly Changing Arctic, *Acoustics Today*, **16**(1), 55-64.

IMPACT/APPLICATIONS

This research is to contribute to further development of a general tool for analysis of propagation, scattering, and reverberation in the complicated Arctic Ocean environments. In particular, it provides a practical way to incorporate advances in modeling of acoustic propagation, and particularly most recent transmission loss (TL) codes based on the Elastic Parabolic Equation (EPE) approximation into arctic reverberation models to improve their prediction capabilities and to allow extremely fast estimations of reverberation in complex ocean environments and waveguides.

RELATED PROJECTS

This research was built on results of previous and current projects on propagation, reverberation and scattering in heterogeneous marine environments funded by ONR-OA and assumed collaboration with Dr. Kevin Williams at APL-UW and other investigators working in this field. This research is also closely related to an effort of Dr. Scott Frank of Marist College on numerical modeling of acoustic propagation in ice-covered environments based an elastic PE approximation.

TECHNOLOGY TRANSFER

Interaction with NRL Stennis: Applying NRL earmuff transducers, originally designed for acoustic characterization of marine sediments, to measuring sound speed in ice samples.

PUBLICATIONS

Anatoliy N. Ivakin and Kevin L. Williams (2020), "Mid-frequency propagation and reverberation time series in a deep ice-covered ocean: Modeling and data analysis", *J. Acoust. Soc. Amer.*, **148**, 2731 (A); doi:10.1121/1.5147587

Andrey Lunkov, Boris Katsnelson, Anatoliy N. Ivakin, and Regina Katsman (2020), "Acoustic propagation and reverberation in shallow water with a gassy bottom: Experiments in the Sea of Galilee and preliminary data analysis", *J. Acoust. Soc. Amer.*, **148**, 2687 (A); doi:10.1121/1.5147440

Anatoliy Ivakin (2019), "A time-domain model of high-frequency backscatter from sea ice with applications to upward looking sonar data analysis", *J. Acoust. Soc. Amer.*, **146**, 3029 (A); doi:10.1121/1.5137502

Scott D. Frank and Anatoliy N. Ivakin (2019), "Application of elastic parabolic equation solutions to calculation of acoustic reverberation in ice-covered underwater environments", POMA: *Proc. Mtgs. Acoust.* **39**, 022002 (2019); doi:10.1121/2.0001210

Scott D. Frank and Anatoliy Ivakin (2019), "Low-frequency reverberation estimates using elastic parabolic equation solutions for ice-covered and ice-free Arctic environments", *J. Acoust. Soc. Amer.*, **146**(3), Pt.2, p.1819 (A); doi:10.1121/1.5068022

A. N. Ivakin (2018), "Backscattering and long-range reverberation in shallow water", in, *Ocean Acoustics,* Proc. L.M. Brekhovskikh's conference, Shirshov Inst. of Oceanology, Moscow: GEOS, pp.114-120.

Anatoliy Ivakin (2018), "A full-field time-domain model for reverberation in complex environments and waveguides with rough interfaces", *J. Acoust. Soc. Amer.*, **144**(3), Pt.2, p.1735 (A); doi:10.1121/1.5067699

Anatoliy Ivakin, Wayne Kreider, and Bonnie Light (2018), "Measurements of sound speed in two types of ice with different microstructure", *J. Acoust. Soc. Amer.*, **144**(3), Pt.2, p.1819 (A); doi:10.1121/1.5068025

Scott D. Frank and A.N. Ivakin (2018), "Long-range reverberation in an Arctic environment: Effects of ice thickness and elasticity", *J. Acoust. Soc. Amer. Express Letters*, **143**(3), EL167-EL173; doi:10.1121/1.5025841

Scott D. Frank and Anatoliy N. Ivakin (2018), "Low-frequency reverberation estimates based on elastic parabolic equation solutions for free-surface and ice-covered Arctic environments", POMA: *Proc. Mtgs. Acoust*. **35**, 005003 (2018); doi:10.1121/2.0000990

Scott D. Frank and Anatoliy Ivakin (2018), "Low-frequency reverberation estimates using elastic parabolic equation solutions for ice-covered and ice-free Arctic environments", *J. Acoust. Soc. Amer.*, **146**(3), Pt.2, p.1819 (A); doi:10.1121/1.5068022

Scott D. Frank and A.N. Ivakin (2017), "Estimating the influence of ice thickness and elasticity on long-range narrow-band reverberation in an Arctic environment", POMA: *Proc. Mtgs. Acoust.*, Volume 30, Issue 1, 070003 (2017); doi:10.1121/2.0000595

Scott D. Frank and A.N. Ivakin (2017), "Estimating the influence of ice thickness and elasticity on long-range narrow-band reverberation in a representative Arctic environment", *J. Acoust. Soc. Amer.*, **141**(5), Pt.2, p.4049 (A); doi:10.1121/1.4989368

A.N. Ivakin (2017), "A full-field scattering coefficient for rough interfaces and a modified sonar equation for long-range reverberation", *J. Acoust. Soc. Amer.*, **142**(4), Pt.2, p.2558 (A); doi:10.1121/1.5014353

A.N. Ivakin (2017), "Physics-based analysis of ULS data: What parameters can be estimated besides the ice draft?", Polar Fridays, APL-UW, 24 March 2017; http://psc.apl.washington.edu/HLD/PolarFridays.html

REPORT DOCUMENTATION PAGE

Form Approved
OMB No. 0704-0188

PLEASE DO NOT RETURN YOUR FORM TO THE ABOVE ADDRESS.

1. REPORT DATE *(DD-MM-YYYY)*	2. REPORT TYPE	3. DATES COVERED *(From - To)*
30-12-2020	Final	1/15/2019-1/14/2020

4. TITLE AND SUBTITLE

Improving prediction of propagation, scattering and reverberation in the Arctic with application to remote acoustic sensing of sea-ice

5a. CONTRACT NUMBER

5b. GRANT NUMBER

N00014-17-1-2196

5c. PROGRAM ELEMENT NUMBER

6. AUTHOR(S)

Ivakin, Anatoliy
Applied Physics Laboratory
University of Washington

5d. PROJECT NUMBER

5e. TASK NUMBER

5f. WORK UNIT NUMBER

7. PERFORMING ORGANIZATION NAME(S) AND ADDRESS(ES)

Applied Physics Laboratory, University of Washington
1013 NE 45th Street
Seattle, WA 98105-6698

8. PERFORMING ORGANIZATION REPORT NUMBER

9. SPONSORING/MONITORING AGENCY NAME(S) AND ADDRESS(ES)

Office of Naval Research
Dr. Kyle Becker
875 N. Randolph Street
Arlington, VA 22203-1995

10. SPONSOR/MONITOR'S ACRONYM(S)

ONR

11. SPONSOR/MONITOR'S REPORT NUMBER(S)

12. DISTRIBUTION/AVAILABILITY STATEMENT

Distribution A: Approved for public release; distribution is unlimited

13. SUPPLEMENTARY NOTES

14. ABSTRACT

A long-term goal is to develop an approach for combining high-frequency short-range upward-looking sonar (ULS) measurements and low-frequency long-range reverberation measurements to provide a wide-area synoptic assessment of ice type distribution. Specific objectives include analysis of two available representative datasets. The first one is comprised of a monostatic 300 kHz ULS echo time series obtained during ICEX03. Its analysis was focused on possible distinguishing between first-year ice and multi-year ice types. The second dataset was obtained during ICEX14 in a deep (3 km) ice-covered ocean using a 3.5 kHz source located at a relatively short range (719m) from receiver. The objective was to suggest a quantitative interpretation of bistatic measurements in the under-ice waveguide including both transmission loss components, relative acoustic intensity of propagation and reverberation time series. Under this project, a combined research was performed, which included theoretical time-domain modeling and computer simulations, laboratory physical modeling and experimentation, data analysis and model-data comparisons.

15. SUBJECT TERMS

Improving prediction of propagation, scattering, and reverberation in the Arctic with application to remote acoustic sensing of sea ice

16. SECURITY CLASSIFICATION OF:			17. LIMITATION OF ABSTRACT	18. NUMBER OF PAGES	19a. NAME OF RESPONSIBLE PERSON
a. REPORT	b. ABSTRACT	c. THIS PAGE			Anatoliy Ivakin
U	U	U	SAR	29	19b. TELEPHONE NUMBER *(Include area code)* 206-616-4808

Reset

Standard Form 298 (Rev. 8/98)
Prescribed by ANSI Std. Z39.18